Plasmonics (2020) 15:1997–2002
https://doi.org/10.1007/s11468-020-01228-1

Resonance Bandwidth Controllable Adjustment of Electromagnetically Induced Transparency-like Using Terahertz Metamaterial

Yuanhao He[1] · Ben-Xin Wang[1] · Pengcheng Lou[1] · Nianxi Xu[2] · Xiaoyi Wang[2] · Yanchao Wang[2]

Received: 27 April 2020 / Accepted: 29 June 2020 / Published online: 6 July 2020

Abstract
In the fields of communication and sensing, resonance bandwidth is a very critical index. It is very meaningful to implement a broadband resonance device with a simple metamaterial structure in the terahertz band. In this paper, we propose a simple metamaterial structure which consists of one horizontal metal strip and two vertical metal strips. This structure can achieve an electromagnetically induced transparency-like (EIT-like) effect in the frequency range of 0.1~3.0 THz to obtain a transparent window with a resonance bandwidth as high as 1.212 THz. When the relative distance between two vertical metal strips is changed, the bandwidth can be effectively controlled. Furthermore, we found that the EIT-like effect can be actively adjusted by replacing vertical metal strips with photosensitive silicon.

Keywords Terahertz metamaterial · Broadband · Electromagnetically induced transparency-like

Introduction

Metamaterial is a kind of artificial composite periodic structure material, which is not found in nature, so it has some characteristics that ordinary materials do not have, including negative refractive index, perfect lensing, and cloaking [1–3]. The properties are mainly caused by its precise geometry and tiny size. Because the tiny structure is smaller than the wavelength it acts on, people can influence the wave through it, so as to achieve the purpose of manipulating electromagnetic waves. These magical properties of metamaterials have attracted the attention of a large number of researchers, and after a lot of research and experiments, metamaterials are widely used in sensors, modulators, optical switches, filters, and other devices [4–15].

The electromagnetically induced transparency (EIT) effect is a quantum interference effect that occurs in a three-level atomic system. When two beams with a frequency close enough and which can be strongly absorbed by the medium at the same time act on the medium together, in a narrow frequency band, the medium suddenly no longer absorbs the beam and becomes transparent [16]. In this transparent band, the dispersion coefficient of the medium increases and the absorption coefficient decreases. Therefore, the EIT effect has potential applications in the slow light [17–19], information storage [20, 21], sensors [22–24], modulators [25–27], filters [28–30], optical switches [31–33], and efficient nonlinear effects [34–36] etc.

In recent years, the research on the use of metamaterials to achieve the EIT effect has attracted widespread attention. In general, we can produce EIT effect through near-field coupling between bright and dark modes [37] or direct coupling between bright and bright modes [38]. But sometimes, we can also generate the phenomenon similar to the EIT effect by means of frequency band superposition which also has the characteristics of the EIT effect, so we call it EIT-like effect.

In addition to the narrow-band and high-Q-factor EIT effect, the wide-band or broadband EIT effect also has potential applications in terms of filters [39] and slow light devices [40]. Some researchers have done some works on the broadband EIT-like effect. For example, Han et al. [41] obtained a tunable ultra-broadband transparent window by adjusting the depth of the asymmetric gap on a self-symmetrical planar metamaterial. This metamaterial structure can be applied to nonlinear optics, filters, sensing, and some other microwave

✉ Ben-Xin Wang
wangbenxin@jiangnan.edu.cn

[1] School of Science, Jiangnan University, Wuxi 214122, China

[2] Key Laboratory of Optical System Advanced Manufacturing Technology, Fine Mechanics and Physics, Chinese Academy of Sciences, Changchun Institute of Optics, Changchun 130033, China

devices. Cheng et al. [42] proposed a chiral metamaterial with triple-layer twisted split-ring resonators structure, which could exhibit a linear polarization conversion as well as asymmetric transmission only for forward and backward propagating linearly polarized waves in a broadband frequency range. The proposed structure also could be beneficial in designing EM wave (optical) isolators, microwave wave plate, or other EM polarization control devices.

In this paper, we propose a simple planar metamaterial structure which consists of one horizontal metal strip and two vertical metal strips. When the electromagnetic wave is incident perpendicularly, an EIT-like effect is achieved, and a transparent window with a bandwidth of 1.212 THz is obtained. Furthermore, the bandwidth of this transparent window can be effectively controlled by adjusting the distance between two vertical metal strips. After research and observation, we found that this type of EIT effect can be actively tuned when the vertical metal strip is replaced with photosensitive silicon of the same size. The proposed EIT-like metamaterial has potential applications in filters, sensors, nonlinear optics, and some other microwave devices.

Structure Design and Method

The structure we proposed consists of one horizontal metal strip and two vertical metal strips, and the material of the metal is gold (Au) with a conductivity of 4.09×10^7 S/m and its thickness is set as 0.3 μm. As shown in Fig. 1a, the entire structure is placed on a silica substrate with a refraction index of 1.5, and the electric field direction of the incident electromagnetic wave is the x direction. Figure 1 b is the unit cell of the proposed structure, and it shows all geometric parameters. The horizontal metal strip (Hms) has the line width of w = 10 μm and the length of l = 120 μm. The vertical metal strips (Vms) have the line width of w = 10 μm and the length of h = 80 μm. The entire structure is symmetrical about the y-axis in the x-direction and symmetrical about the x-axis in the y-direction. The distance between two metal bars is l_1 = 70 μm, and the distance between the left metal bar and the left of the horizontal metal bar is l_2 = 15 μm. In order to obtain accurate results, the finite difference time domain method (FDTD) is utilized. In the specific calculation, the plane electromagnetic wave has x polarization direction. We set the boundary conditions as periodic boundary in X-Y direction and perfectly matched layers in Z direction.

Result and Discussion

Figure 2 is the resonance response of the metamaterial structure, and we can find that the frequency range of the entire resonance spectrum is 0.1~3.0 THz. There are two resonance dips D1 and D2 in the resonance spectrum. The resonance dip D1 on the left is slightly wider and its resonance frequency is 0.732 THz, while the resonance dip D2 on the right is slightly sharp and its resonance frequency is 2.196 THz. A broad transparent window with a high full width at half maximum of 1.212 THz appears between these two dips. The transmittance of these two resonance dips are very close to 0, and the transmittance of the transparent window peak exceeds 90%. According to the proposed metamaterial structure, we obtain a transparent window with an ultra-wide band with good performance.

In order to explain the reason for the two resonance dips on the resonance spectrum and the mechanism of the ultra-broadband transparent window, we give the electric field distributions (|E| and Ez) of the two resonance dips at their resonance frequencies. From Fig. 3 a and c, we can find that the electric field distribution is symmetrical about the y-axis in the x direction, the electric field is evenly distributed on the left and right sides of the structure, and the electric field on the left is an electric field composed of positive charges, and the electric field on the right is composed of negative charges, so the electric field is a typical dipole electric field. Obviously, dip

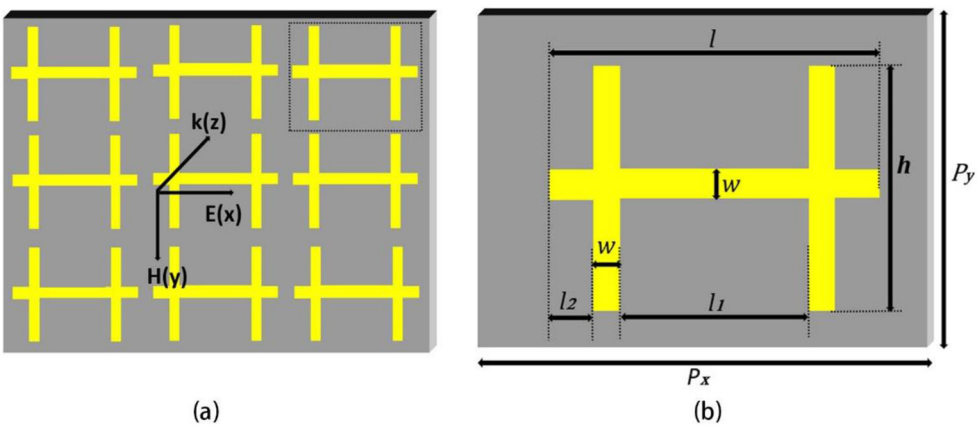

Fig. 1 **a** The multiple-unit structure on the substrate, and the incident direction and polarization state of electromagnetic waves are also shown. **b** Unit cell of the proposed structure, the relevant dimensions are as follows: p_x = 150 μm, p_y = 90 μm, l = 120 μm, h = 80 μm, l_1 = 70 μm, w = 10 μm

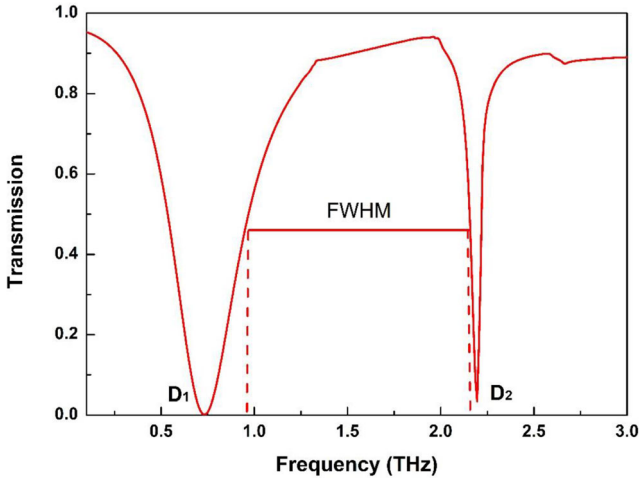

Fig. 2 Transmission spectrum of the designed structure

D1 is generated by the dipole resonance formed on the left and right sides of the structure.

As shown in Fig. 3 b and d, the electric field is distributed at the bottom of the three metal strips, but the electric field at the two ends of the metal horizontal strip is very strong, and the electric field at the ends of the two vertical metal strips is slightly weaker. It is worth noting that the electric field at the left end of the horizontal metal strips is generated by positive charges, and the electric field at the right end is generated by negative charges, so it can be regarded as a dipole. The electric field of the left vertical metal strip is generated by negative charges, which is opposed to the electric field generated by positive charge on the left side of the horizontal metal strip. Therefore, the two ends of the left vertical metal strip and the left side of the horizontal metal strip exactly constitute an electric quadrupole.

Similarly, the electric field at both ends of the right vertical metal strip is generated by positive charges, which is opposite to the electric field generated by negative charge at the right side of the horizontal metal strips. The two ends of the right vertical metal strips and the right side of the horizontal metal strip also form an electric quadrupole. So, dip D2 is generated by the coupling of the formed dipole and two electrical quadrupoles. The superposition of the two resonances produces an ultra-broadband transparent window. Because it is different from the traditional EIT effect caused by the direct superposition of these two resonances, we call this phenomenon EIT-like effect.

We find that when the length of l keeps constant and only the lengths of l_2 or l_1 change, the ultra-broadband transparent window will change significantly. As shown in Fig. 4, when we gradually increase the length of l_2 from 15 to 45 μm, we can find that the linewidth of Dip D1 not changed, but its resonance frequency changes resulting in a blue shift. It is worth noting that the linewidth of Dip D2 has increased significantly, and the resonance frequency also changes significantly resulting in a red shift. The transmittance peak of the transparent window increases slightly. As shown in Fig. 5a, when the length of l_2 equal to 45 μm, the entire resonance curve becomes an ordinary narrow-band EIT resonance curve, so that we achieve the control to the bandwidth of the transparent window. Figure 5b–e show the electric field |E| distributions (|E| and Ez) at the frequency of D3 and D4. From Fig. 5b, we can see that the electric field is strongly distributed in the two sides of the horizontal metal strips and between the two vertical metal strips. As shown in Fig. 5d, the electric field on the left is composed of positive charges, and the electric field on the right is composed of negative charges, so the electric field is still a typical dipole electric field, and it means

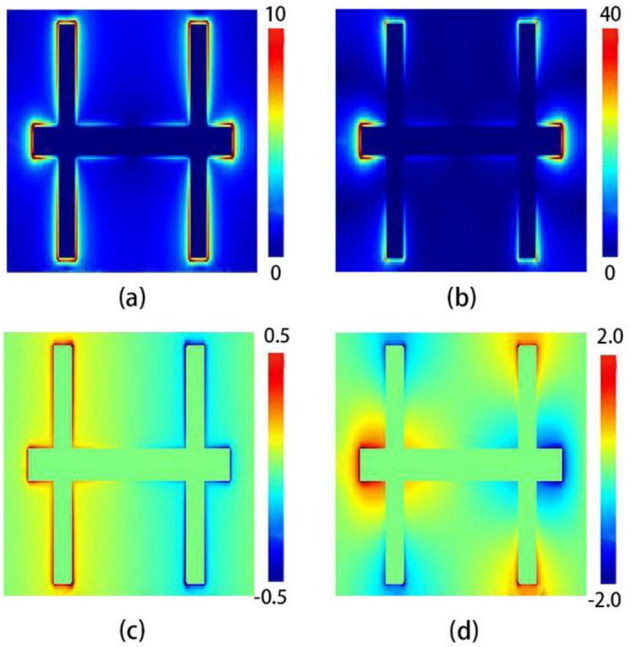

Fig. 3 **a**, **b** The |E| distributions of the resonance dips D1 and D2. **c**, **d** The real Ez distributions of D1 and D2

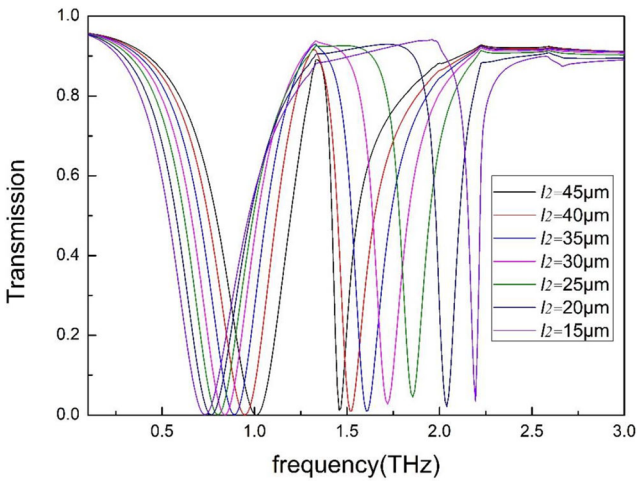

Fig. 4 Transmission spectra when l_2 equal to 15 μm, 20 μm, 25 μm, 30 μm, 35 μm 40 μm, and 45 μm, respectively

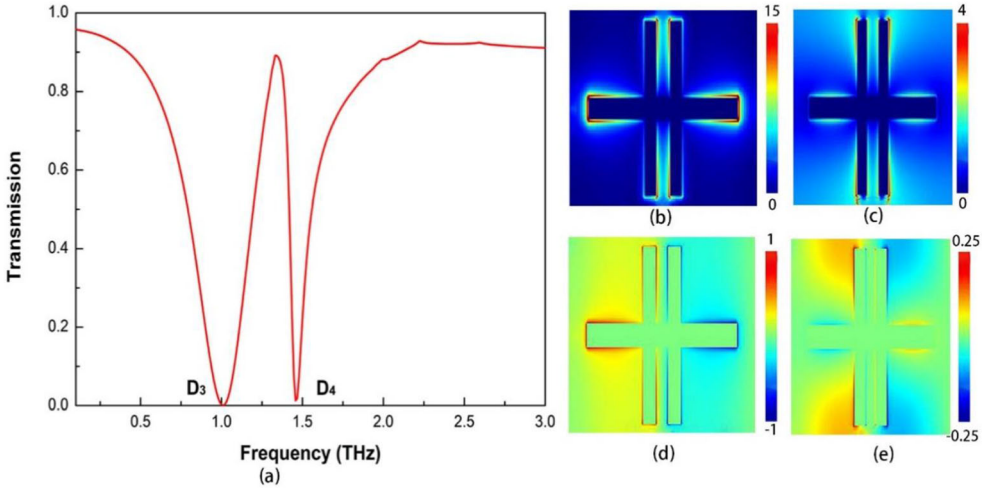

Fig. 5 **a** The transmission spectra when l_2 equal to 45 μm. **b**, **c** The |E| distributions of the resonance dips D3 and D4. **d**, **e** The real Ez distributions of Dips D3 and D4

that it forms a dipole. In Fig. 5c, we can see that the electric field is distributed mainly on the two sides of two vertical metal strips, and a little on the sides of horizontal metal strip. As shown in Fig. 5e, the electric field of the left vertical metal strip is produced by positive charges, which is opposed to the electric field produced by negative charges on the left side of the horizontal metal strip. Therefore, the two ends of the left vertical metal strip and the left side of the horizontal metal strip form an electric quadrupole. Similarly, an electric quadrupole is formed on the right side of the structure, and the dipole and two quadrupoles are coupled to produce D4, and the superposition of the two resonances produces the transparent window in Fig. 5a.

When the length of l_2 increases from 15 to 45 μm, and the length of l_1 decreases accordingly, that is, the common length between the dipoles decreases. Since the resonance frequency of the electric dipole is inversely proportional to it, the decreases of distance between them results in an increase in the resonance frequency. This is the reason why the resonance frequency of D3 becomes larger and the blue shift occurs relative to D1. The increase of l_2 increases the equivalent length of the electric quadrupole, and the resonance frequency of the electric quadrupole is inversely proportional to its equivalent length. In this way, the resonance frequency of the electric quadrupole decreases, and after the electric dipole's excitation and coupling, the resonance frequency of D4 also decreases relative to D2, and the red shift occurs. After superposition between the two resonances, the transparent window becomes narrow.

We found that when the parameter l_2 changes, the frequencies of Dip D3 and D4 change accordingly, which results in a significant change in the width of the transparent window. We give the proportional relationship between the length of l_2 and the full width at half maximum (FWHM) of the transparent window.

From Fig. 6, we can find that when l_2 gradually changes from 15 to 45 μm, the full width at half maximum of the transparent window also changes accordingly. In the figure, the FWHM and the length of l_2 show a linear relationship, and their ratio is roughly a straight line. With this relationship, we can get the desired FWHM by setting the length of l_2.

Photosensitive silicon is a material whose conductivity is changed by external laser stimulation. Using it we can achieve dynamic regulation of many optoelectronic devices. We replaced the metal dielectric gold of the two vertical metal strips in the structure with photosensitive silicon, keeping other parameters unchanged, and then observed the resonance response. From Fig. 7, we can find that when we apply laser stimulation to make the photosensitive silicon have a conductivity of 100 S/m, no matter how the length of l_2 changes, there is only one resonance response in the transmission spectrum, which is very stable, but when we add laser stimulation to make the photosensitive silicon when the electrical conductivity of is 4.09×10^7 S/m, two resonance dips and a transparent window appear, and the transmission spectrum at this time is exactly the same as the transmission spectrum in Fig. 4. This

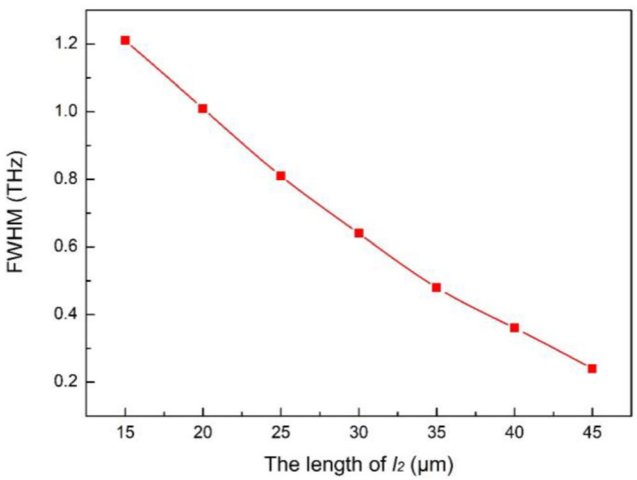

Fig. 6 The relationship between the length of l_2 and the full width at half maximum (FWHM) of the transparent window

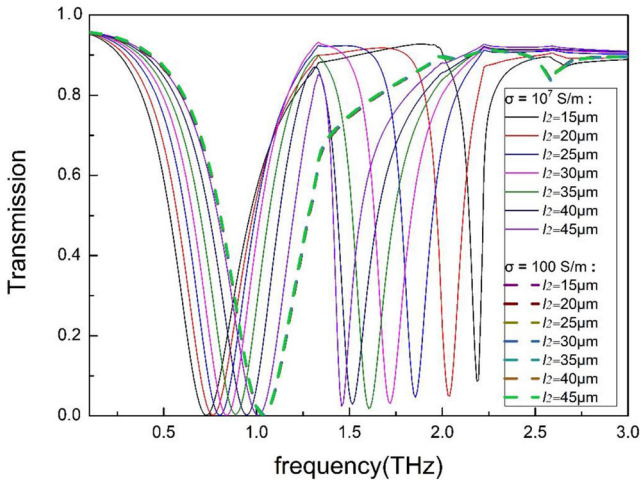

Fig. 7 The transmission spectrum when the conductivity of photosensitive silicon is 100 s/m and 10^7 s/m, and the length of l_2 is increased from 15 to 45 μm

shows that by using photosensitive silicon, our structure can also achieve the dynamic regulation of resonance, which is very meaningful for the design of many optoelectronic devices such as light switching and modulators.

Conclusion

In conclusion, a metamaterial structure consisted of one horizontal metal strip and two vertical metal strips is demonstrated, and the structure can realize a wide bandwidth EIT-like transparent window whose full width at half maximum (FWHM) can reach to 1.212 THz. By changing the l_2 parameter, the FWHM of the transparent window can be adjusted obviously. In addition, we replaced the material of the two metal strips with photosensitive silicon to achieve active regulation of the resonance response. This structure has potential application value in sensors, modulators, optical switches, filters, and so on.

Acknowledgments This research was funded by the National Natural Science Foundation of China (11647143), Natural Science Foundation of Jiangsu (BK20160189), China Postdoctoral Science Foundation (2019 M651692), Jiangsu Postdoctoral Science Foundation (2018K113C), and Fundamental Research Funds for Central Universities (JUSRP51721B).

References

1. Suzuki T, Sekiya M, Sato T, Takebayashi Y (2018) Negative refractive index metamaterial with high transmission, low reflection, and low loss in the terahertz waveband. Opt Express 26:8314–8324
2. Rosenblatt G, Orenstein M (2015) Perfect lensing by a single interface: defying loss and bandwidth limitations of metamaterials. Phys Rev Lett 115:195504
3. Schurig D, Mock JJ, Justice BJ, Cummer SA, Pendry JB, Starr AF, Smith DR (2006) Metamaterial electromagnetic cloak at microwave frequencies. Science 314:977–980
4. Schueler M, Mandel C, Puentes M, Jakoby R (2012) Metamaterial inspired microwave sensors. IEEE Microw Mag 13:57–68
5. Wang BX, Tang C, Niu Q, He Y, Chen T (2019) Design of narrow discrete distances of dual−/triple-band terahertz metamaterial absorbers. Nanoscale Res Lett 14:64
6. Keshavarz A, Vafapour Z (2019) Sensing avian influenza viruses using terahertz metamaterial reflector. IEEE Sensors J 19:5161–5166
7. Chen HT, Padilla WJ, Cich MJ, Azad AK, Averitt RD, Taylor AJ (2009) A metamaterial solid-state terahertz phase modulator. Nat Photonics 3(3):148–151
8. Wang BX (2017) Quad-band terahertz metamaterial absorber based on the combining of the dipole and quadrupole resonances of two SRRs. IEEE J Sel Top Quantum Electron 23:4700107
9. Wang BX, Wang GZ, Sang T (2016) Simple design of novel triple-band terahertz metamaterial absorber for sensing application. J Phys D Appl Phys 49:165307
10. Wang BX, Wang GZ, Wang LL (2016) Design of a novel dual-band terahertz metamaterial absorber. Plasmonics 11:523–530
11. Nikolaenko AE, Papasimakis N, Chipouline A, De Angelis F, Di Fabrizio E, Zheludev NI (2012) THz bandwidth optical switching with carbon nanotube metamaterial. Opt Express 20:6068–6079
12. Wang BX, He Y, Lou P, Xing W (2020) Design of a dual-band terahertz metamaterial absorber using two identical square patches for sensing application. Nanoscale Adv 2:763–769
13. García-García J, Bonache J, Gil I, Martín F, Velazquez-Ahumada MC, Martel J (2006) Miniaturized microstrip and CPW filters using coupled metamaterial resonators. IEEE Trans Microw Theory Tech 54:2628–2635
14. Wang BX, Wang GZ, Wang LL, Zhai X (2016) Design of a five-band terahertz absorber based on three nested split-ring resonators. IEEE Photon Technol Lett 28:307–310
15. Cheben P, Čtyroký J, Schmid JH, Wang S, Lapointe J, Wangüemert-Pérez JG et al (2019) Bragg filter bandwidth engineering in subwavelength grating metamaterial waveguides. Opt Lett 44:1043–1046
16. Fleischhauer M, Imamoglu A, Marangos JP (2005) Electromagnetically induced transparency: optics in coherent media. Rev Mod Phys 77:633–673
17. Khurgin JB (2005) Optical buffers based on slow light in electromagnetically induced transparent media and coupled resonator structures: comparative analysis. J Opt Soc Am B 22:1062–1074
18. Zhang J, Hernandez G, Zhu Y (2008) Slow light with cavity electromagnetically induced transparency. Opt Lett 33:46–48
19. Liu T, Wang H, Liu Y, Xiao L, Zhou C, Liu Y, Xu C, Xiao S (2018) Independently tunable dual-spectral electromagnetically induced transparency in a terahertz metal–graphene metamaterial. J Phys D Appl Phys 51:415105
20. Heinze G, Hubrich C, Halfmann T (2013) Stopped light and image storage by electromagnetically induced transparency up to the regime of one minute. Phys Rev Lett 111:033601
21. Hsu MT, Hetet G, Gloeckl O, Longdell JJ, Buchler BC, Bachor HA, Lam PK (2006) Quantum study of information delay in electromagnetically induced transparency. Phys Rev Lett 97:183601
22. Meng FY, Wu Q, Erni D, Wu K, Lee JC (2012) Polarization-independent metamaterial analog of electromagnetically induced transparency for a refractive-index-based sensor. IEEE Trans Microw Theory Tech 60:3013–3022
23. Yadipour R, Abbasian K, Rostami A, Koozekanani ZD (2007) A novel proposal for ultra-high resolution and compact optical displacement sensor based on electromagnetically induced transparency in ring resonator. Prog Electromagn Res 77:149–170

24. Liu T, Wang H, Liu Y, Xiao L, Yi Z, Zhou C, Xiao S (2018) Active manipulation of electromagnetically induced transparency in a terahertz hybrid metamaterial. Opt Commun 426:629–634
25. Paternostro M, Kim MS, Ham BS (2003) Generation of entangled coherent states via cross-phase-modulation in a double electromagnetically induced transparency regime. Phys Rev A 67:023811
26. Xiao S, Wang T, Liu T, Yan X, Li Z, Xu C (2018) Active modulation of electromagnetically induced transparency analogue in terahertz hybrid metal-graphene metamaterials. Carbon 126:271–278
27. Zografopoulos DC, Swillam M, Beccherelli R (2016) Hybrid plasmonic modulators and filters based on electromagnetically induced transparency. IEEE Photon Technol Lett 28(7):818–821
28. Lu H, Liu X, Wang G, Mao D (2012) Tunable high-channel-count bandpass plasmonic filters based on an analogue of electromagnetically induced transparency. Nanotechnology 23:444003
29. Davanço M, Holmstrom P, Blumenthal DJ, Thylén L (2003) Directional coupler wavelength filters based on waveguides exhibiting electromagnetically induced transparency. IEEE J Quantum Electron 39:608–613
30. Jeong T, Bae IH, Moon HS (2017) Noise filtering via electromagnetically induced transparency. Opt Commun 383:31–35
31. Schmidt H, Ram RJ (2000) All-optical wavelength converter and switch based on electromagnetically induced transparency. Appl Phys Lett 76:3173–3175
32. Clarke J, Chen H, van Wijngaarden WA (2001) Electromagnetically induced transparency and optical switching in a rubidium cascade system. Appl Opt 40:2047–2051
33. Rao S, Hu X, Xu J, Li L (2017) Optical switching of cross intensity correlation in cavity electromagnetically induced transparency. J Phys B Atomic Mol Phys 50(5):055504
34. Harris SE, Field JE, Imamoğlu A (1990) Nonlinear optical processes using electromagnetically induced transparency. Phys Rev Lett 64:1107–1110
35. Zhang GZ, Hakuta K, Stoicheff BP (1993) Nonlinear optical generation using electromagnetically induced transparency in atomic hydrogen. Phys Rev Lett 71(19):3099–3102
36. Hao L, Xue Y, Fan J, Jiao Y, Zhao J, Jia S (2019) Nonlinearity of microwave electric field coupled Rydberg electromagnetically induced transparency and Autler-Townes splitting. Appl Sci 9:1720
37. Hu S, Yang HL, Chen J, & Huang XJ (2016) Study of dual-spectral electromagnetically induced transparency in bright-dark mode coupling metamaterials. In 2016 11th International Symposium on Antennas, Propagation and EM Theory (ISAPE). IEEE, (pp. 488-491)
38. Yahiaoui R, Burrow JA, Mekonen SM, Sarangan A, Mathews J, Agha I, Searles TA (2018) Electromagnetically induced transparency control in terahertz metasurfaces based on bright-bright mode coupling. Phys Rev B 97:155403
39. Hu S, Liu D, Lin H, Chen J, Yi Y, Yang H (2017) Analogue of ultra-broadband and polarization-independent electromagnetically induced transparency using planar metamaterial. J Appl Phys 121:123103
40. Wu C, Khanikaev AB, Shvets G (2011) Broadband slow light metamaterial based on a double-continuum Fano resonance. Phys Rev Lett 106:107403
41. Han S, Yang H, Guo L (2013) Ultra-broadband electromagnetically induced transparency using tunable self-asymmetric planar metamaterials. J Appl Phys 114:163507
42. Cheng YZ, Nie Y, Cheng ZZ, Wu L, Wang X, Gong RZ (2013) Broadband transparent metamaterial linear polarization transformer based on triple-split-ring resonators. J Electromagn Waves Appl 27:1850–1858